Delaying the buzz onset in a supersonic inlet by multi-row disk concept

Sohrab Panahandeh Taghi-Abad , Mohammad Hossein Moghimi Esfand-Abadi ,
Javad Sepahi-Younsi *

Mechanical Engineering Department, Faculty of Engineering, Ferdowsi University of Mashhad, P.O. Box 91775-1111, Mashhad, Iran

ARTICLE INFO

ABSTRACT

At subcritical operating conditions of the supersonic air inlets, if the mass flow rate drops below a certain threshold for any reason, the shock waves begin to oscillate back and forth through the inlet, causing the inlet to become unstable. This event is known as the buzz phenomenon. A literature review reveals that one of the proposed methods for improving the inlet stability is using the Multi-Row Disk (MRD) arrangement concept. In this method, part of the inlet compression body is replaced with a series of disks, and between these disks, a series of cavities are created that can prevent flow separation. The use of this method is novel and very limited studies have been conducted on it so far. Most of the studies have focused on the effects of the size and number of cavities that are created between the disks on the inlet performance parameters, and no research has been done about the inlet stability and buzz phenomenon. Therefore, the main goal of the present study is to investigate the effects of MRD method on preventing and postponing the buzz phenomenon. In this research, an axisymmetric supersonic inlet is computationally studied at a free stream Mach number of 2. The Reynolds-Averaged Navier-Stokes (RANS) equations are solved in an unsteady state and the k-ω turbulence model is used to account for the turbulence effects. The results showed that MRD method can delay the buzz onset and increase the subcritical stability margin of the inlet significantly. In addition, this method, relying on simple geometric principles, not requiring complex control systems, and not adversely affecting the inlet performance parameters, can improve the inlet stability by decreasing the amplitude and frequency of the buzz oscillations.

1. Introduction

All aerospace vehicles require a propulsion system to carry out their flight missions. Among these, aircrafts and some missiles use air-breathing engines to generate the required thrust. The design of supersonic air inlets must be such that, in addition to delivering the required mass flow to the engine, they have the least total pressure loss and external drag [1]. For a supersonic inlet, depending on the flight conditions, three operating modes can be distinguished based on the location of the terminal normal shock wave relative to the inlet throat [2]. These three operating modes are supercritical, critical, and subcritical operating conditions [3]. If the normal shock wave is located downstream of the throat, it is a supercritical operating mode; if it is exactly at the throat, it is a critical operating mode; and if it is upstream of the throat, it is a subcritical operating mode [4].

When the inlet back pressure is relatively low, the terminal normal shock is located downstream of the throat. In this case, the normal shock is relatively strong, resulting in low total pressure recovery (defined as

the ratio of the total pressure at the inlet exit to the freestream total pressure). Additionally, in this condition, the intersection of oblique shocks with the cowl lip or nearby surfaces leads to minimal spillage of the incoming flow [5]. When the back pressure increases sufficiently, the terminal normal shock moves upstream and stands at the inlet throat, where it is at its weakest situation. This condition is referred to as the critical operating mode, characterized by maximum total pressure recovery and maximum mass flow rate [5]. With a further increase in back pressure, the terminal normal shock moves upstream of the throat and stands outside the inlet. This condition is defined as the subcritical operating mode. Because this external shock is stronger than the one formed at the throat, the inlet experiences greater total pressure losses. Moreover, as the shock system moves away from the cowl lip, flow spillage increases, leading to a decrease in the captured mass flow rate [5].

The critical operating mode is considered the most optimal condition for a supersonic inlet, as it ensures maximum total pressure recovery and maximum mass flow rate. While the critical condition offers optimal performance, in practical applications the inlet may transition into the
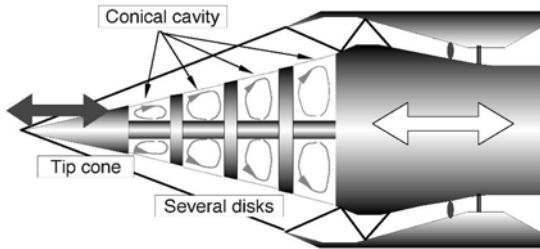

Fig. 1. Inlet with MRD concept [18].

subcritical regime, especially under increased back pressure or engine-induced disturbances. In subcritical mode, if the mass flow ratio falls below a certain threshold, the inlet becomes unstable and the buzz phenomenon may occur [6]. Buzz is the most prominent indicator of inlet flow instability, characterized by continuous oscillations of the shock system and the mass flow rate, accompanied by significant total pressure loss.

The buzz phenomenon is driven by the interaction of the terminal normal shock with upstream oblique shocks and the boundary layer on the spike, which induces flow separation near the inlet)a key factor in the onset of buzz ([7]. The occurrence of these oscillations causes problems in engine structures and reduces the engine thrust. If the amplitude of the oscillations is large, it can cause combustion failure and consequently the failure of the flying vehicle's engine [8].

There are two main criteria to describe the onset of the buzz phenomenon, known as the Ferri and Dailey criteria. Ferri criterion defines the starting point of the buzz phenomenon as the collision of the vortex sheet (resulting from the intersection of the oblique shock wave with the normal shock wave) with the boundary layer inside the cowl, which causes the flow separation and choking at the inlet throat [9]. The other criterion, which is called Dailey, states that the cause of buzz initiation is the separation of the boundary layer over the spike surface resulting from the interaction of the normal shock wave with the boundary layer on the spike [10].

Considering that the main cause of buzz in both criteria is the separation of the boundary layer, therefore, by controlling the separation, the buzz phenomenon can be suppressed [9,10]. To control the boundary layer and prevent flow separation caused by the interaction of shock waves with the boundary layer, many methods have been researched and investigated, which are plasma actuator, boundary layer suction, fluid injection into the boundary layer, vortex generator, micro ramps, and flow separator [11].

Shigematsu et al. in 1991 numerically simulated the effects of a cavity on the stability of a mixed-compression supersonic air inlet. The location of the cavity in their study was in the throat section of the inlet. They showed that the cavity increases the optimal pressure gradient and prevents flow separation. Their results also showed that by creating a cavity in the inlet, the normal shock wave stands at the trailing edge of the cavity, increasing total pressure recovery and postponing the buzz phenomenon [12].

Vyas et al. in 2011, in an experimental study, investigated the effects of vortex generators on a supersonic inlet. They showed that vortex generators are effective in stabilizing shock waves and postponing the buzz phenomenon. The location of vortex generators affects the stability of shock waves, but they cause a reduction in pressure recovery [13].

Jagannathan and Johansson in 2019 investigated the effects of energy injection through nanoparticles into the boundary layer of the spike of a supersonic inlet for free stream Mach number of 2 on the onset of the buzz phenomenon. Their results showed that applying energy injection upstream of the inlet had no effect on postponing the buzz phenomenon and it reduced the stability of the inlet. They also showed that the injection of nanoparticles downstream of the throat at the subsonic diffuser is effective in improving the inlet performance [14].

Sepahi and Maadi in 2022, by examining and comparing two mixed-compression supersonic inlets with porous and slot boundary layer bleeds, found that using a porous bleed results in better inlet performance and increases mass flow ratio and total pressure recovery more, while flow distortion is reduced. They showed that the main advantage
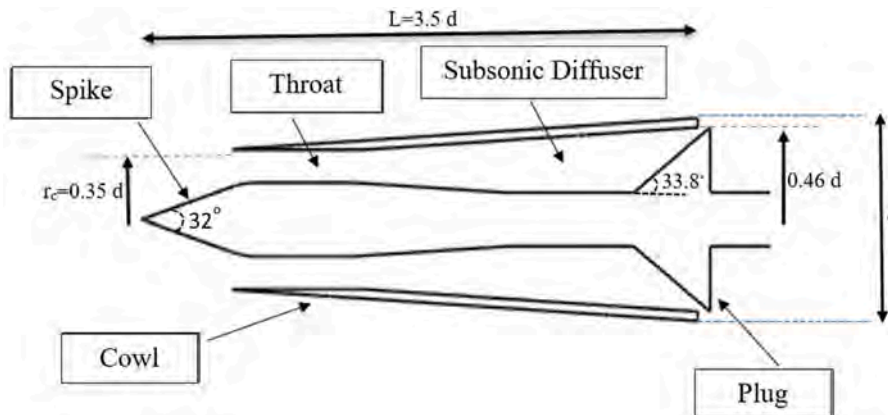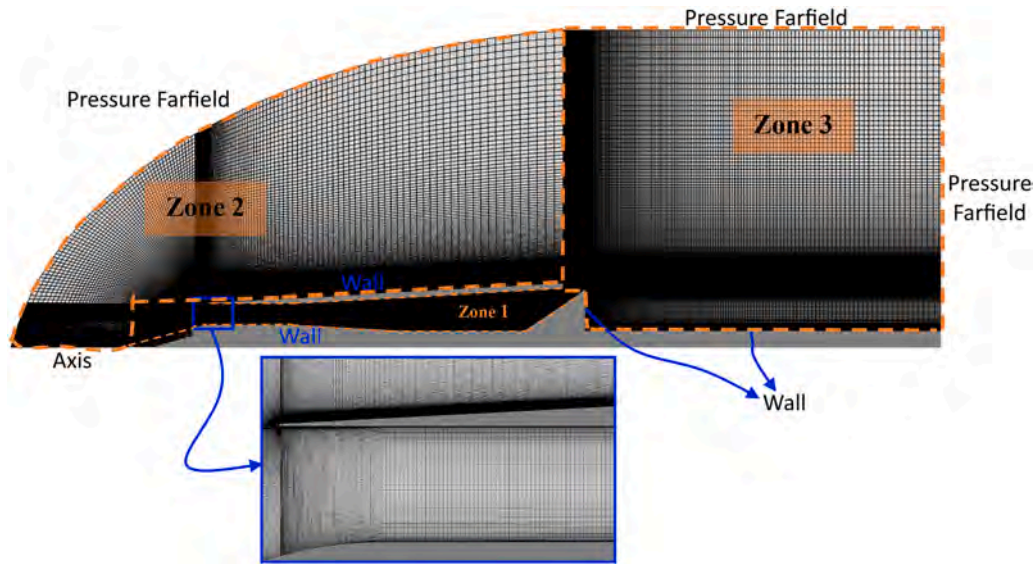

Fig. 2. Inlet model side view.

Fig. 3. Computational domain and boundary conditions.

Table 1
Percentage of cells in each zone that meet mesh quality criteria.

Zone Name	Number of Cells	Aspect Ratio	Max./ Min. Aspect Ratio	Skewness	Max./Min. Skewness
Zone 1	67,282	91 % of Cells<10	8/1	97 % of Cells<0.25	0.33/0
Zone 2	31,277	90 % of Cells<10	16/1	95 % of Cells<0.25	0.41/0
Zone 3	29,450	93 % of Cells<10	24/1	99 % of Cells<0.25	0.44/0

of the slot blade is in further delaying the buzz phenomenon as compared with the porous bleed [15].

Sepahi and Esmaeili in 2023 conducted a numerical study of the buzz phenomenon in an external-compression supersonic inlet for free stream Mach number of 2. Their results showed that neither the Ferri criterion nor the Daily criterion was responsible for the onset of buzz and the separated and reversed flow near the inner surface of the cowl is the main cause of the buzz onset [16].

Chen et al. introduced an innovative approach in 2019 by creating narrow slots on the compression surface of a rectangular inlet. These slots transfer the separation region to the external environment due to pressure differences, delaying flow separation and the buzz onset. The

main advantage of this method is that, with the presence of these thin slots, the boundary layer suction is performed as needed and according to the arrangement of the shock waves. Therefore, the mass flow rate removed from the inlet main flow is much less compared to the typical boundary layer suction method [17].

The MRD idea was first proposed in 2002 in Japan by Kobayashi [18]. In this concept as seen from Fig. 1, the inlet features a center body consisting of a tip cone followed by a series of disks. The space between these disks creates a series of cavities that help control the boundary layer on the compression surface. The initial goal of this idea was to create the conditions of variable geometry for the inlet by adjusting the distance between the disks. It was discovered that the MRD method enhances the inlet performance at off-design conditions [19].

Kobayashi et al. used the MRD idea to reduce the drag of an aerospike body in 2007 [20]. They experimentally demonstrated that by increasing the number of disks in front of the aerospike, not only the drag force can be reduced, but also the boundary layer thickness downstream of the cavities and the flow oscillations inside the cavities can be decreased [21]. Similarly, Esmailzadeh Vali and Abbasi in 2022 performed a numerical analysis on a blunt body featuring the multi-row disk method at a hypersonic speed, revealing that this method reduces drag coefficient and aerodynamic heating on the body surface [22].

In 2023, Sinha et al. numerically investigated the effects of the tip cone angle in a spike-like body equipped with MRD. By analyzing the flow field inside the cavities, they concluded that among the three angles of 12, 15, and 20 degrees for the half-cone angle, the 20-degree angle is
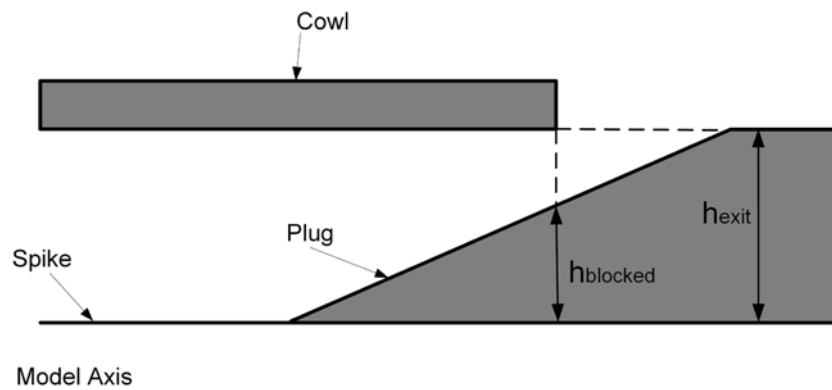

Fig. 4. Schematic of the inlet and plug geometry at the end of the model [28].

Table 2

Summary of supersonic inlet operating modes and their associated flow characteristics according to the values of EBR.

EBR Range	Stability	Shock Location Relative to the Throat	Operating Condition	Flow Behavior
<60.0 %	Stable	Downstream	Supercritical	Low Pressure Recovery, Maximum Mass Flow Rate
60.0 %– 62.5 %	Stable	at the Throat	Critical	High Pressure Recovery, Maximum Mass Flow Rate
62.5 %– 67.5 %	Local Oscillations [30]	Slightly Upstream	Subcritical	Low Pressure Recovery, Drop in Mass Flow Rate
>67.5 %	Unstable	Oscillation at Upstream	Mixed Condition (Buzz)	Severe Pressure Loss, Mass Flow Oscillation
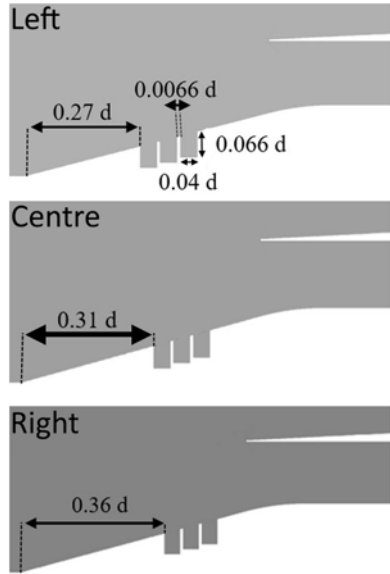
Fig. 5. Geometric details of the first MRD configuration.

better at Mach number 2 according to the values of drag coefficients and compression efficiencies [23].

As seen and to the authors' knowledge, only two papers have examined the effects of the MRD method on air inlets, while in other studies this method has been mainly used to reduce the drag of a spike-like object. Additionally, it is observed that in those two studies, the impacts of MRD on inlet performance were investigated, and so far, no study has examined the effects of MRD on the buzz phenomenon and inlet stability. Therefore, the primary objective of the present study is to investigate the buzz phenomenon in the presence of the MRD method and to examine its impacts on delaying the buzz phenomenon. In this research, a numerical study as well as an analysis of an axisymmetric supersonic inlet under subcritical operating conditions have been conducted, and performance parameters and the buzz phenomenon have been investigated. The freestream Mach number, static pressure, and static temperature were 2, 10,555 Pa, and 168 K, respectively, which are consistent with the wind tunnel data used for code validation. Additionally, a turbulence intensity of 2.5 %, based on the wind tunnel data, was applied.

2. Numerical methodology

The time-dependent Reynolds-Averaged Navier-Stokes (RANS) equations are solved in this research using a computational code previously created by the authors [24–28]. In this study, the integral form of the governing equations, excluding body forces, was utilized:

$$\frac{\partial}{\partial t} \iint_A \vec{W} dA + \int_s \vec{F}_c ds + \alpha \iint_A \vec{V}_c dA = \int_s \vec{F}_v ds + \alpha \iint_A \vec{V}_v dA \tag{1}$$

$$\vec{W} = \begin{bmatrix} \rho \\ \rho u \\ \rho v \\ \rho E \end{bmatrix}, \vec{F}_c = \begin{bmatrix} \rho V_n \\ \rho u V_n + n_x P \\ \rho v V_n + n_r P \\ \rho H V_n \end{bmatrix}, \vec{F}_v = \begin{bmatrix} 0 \\ n_x \tau_{xx} + n_r \tau_{xr} \\ n_x \tau_{xr} + n_r \tau_{rr} \\ n_x \theta_x + n_r \theta_r \end{bmatrix}, \vec{V}_c$$

$$= \frac{1}{r} \begin{bmatrix} \rho v \\ \rho u v \\ \rho v^2 \\ \rho v H \end{bmatrix}, \vec{V}_v = \frac{1}{r} \begin{bmatrix} 0 \\ \tau_{xr} \\ \tau_{rr} - \tau_{\theta\theta} \\ u\tau_{xr} + v\tau_{rr} + k\left(\frac{\partial T}{\partial r}\right) \end{bmatrix} \tag{2}$$

$$V_n = \vec{V} \cdot \vec{n} = n_x u + n_r v$$

$$n_x = \frac{\Delta r}{\Delta s}, n_r = -\frac{\Delta x}{\Delta s}, \Delta s = \sqrt{\left(\Delta x^2 + \Delta r^2\right)}$$

$$\theta_x = u\tau_{xx} + v\tau_{xr} + k\frac{\partial T}{\partial x} \tag{3}$$

$$\theta_r = u\tau_{xr} + v\tau_{rr} + k\frac{\partial T}{\partial r}$$

E and H represent the total energy and total enthalpy per unit mass,
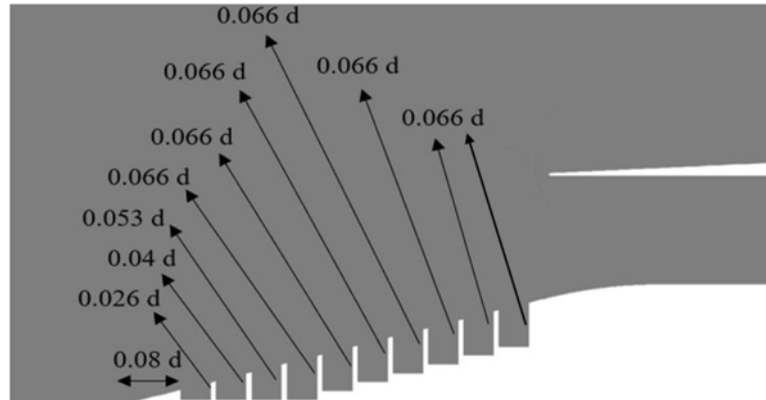
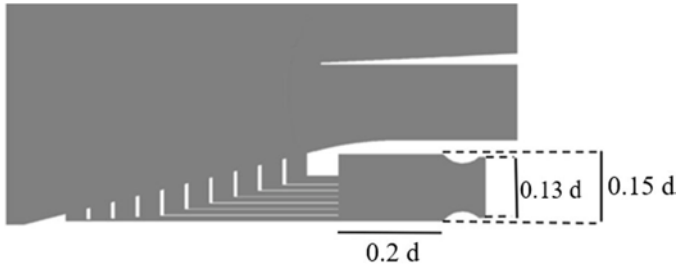**Fig. 6.** Geometric details of the second MRD configuration.

Fig. 7. Geometric details of the third MRD configuration.

respectively. The variable α equals 1 for axisymmetric flow and 0 for planar flow. Δs denotes the length of the two-dimensional cell face, A indicates the area of the computational cell, and V_n refers to the velocity component perpendicular to the cell face. These equations have been discretized utilizing the finite volume method. The convective fluxes are calculated using the Roe scheme, which employs a second-order accurate MUSCL (monotone upstream-centered schemes for conservation laws) approach. For time advancement and temporal discretization, a four-stage Runge-Kutta integration method is applied. Given that the inlet geometry is axisymmetric and the flow angle of attack is zero, a two-dimensional model with an axis boundary condition is utilized to reduce both time and computational costs. The SST (Shear Stress Transport) k-ω turbulence model is employed in this research because of its remarkable capability to accurately predict the initiation and extent of flow separation in conditions with adverse pressure gradients while minimizing computational costs. Air is treated as an ideal gas, and its molecular viscosity is calculated using the Sutherland viscosity law. For unsteady cases, 50 iterations are performed per each time step, while the time step is selected to be 5×10^{-6} s. This time step value was chosen based on our previous studies about inlets and according to the solution independence from time step size.

2.1. Inlet model

The schematic representation of the geometry and dimensions of the inlet under study is illustrated in Fig. 2. The inlet is axisymmetric and mixed-compression that has been designed for the free stream Mach number of 2. To enhance the mesh quality, several computational blocks have been utilized within the domain to create a structured grid.

Considering the critical role of flow separation on the buzz onset, the mesh has been refined near the walls to capture separation more precisely. In addition, the computational domain has been extended by one inlet length behind the inlet to prevent the use of the pressure outlet boundary condition and the application of a specific static pressure at the end of the inlet, and to allow the free oscillation of the flow within the inlet. Fig. 3 illustrates the details of the mesh and the boundary conditions applied.

Fig. 3 shows the division of the domain into three zones. Table 1, presents the mesh quality parameters and number of cells for each zone. It is noted that Zone 1 represents the inner part of the inlet. To better evaluate the mesh quality, for each zone the minimum and maximum values of aspect ratio and skewness, as well as the percentage of cells that satisfy common quality thresholds, have been reported. According to this table, the mesh exhibits suitable quality for the current simulation.

For validation of the numerical methodology, the wind tunnel data of the current inlet has been used [29]. To adjust the inlet back pressure in the experimental model and to achieve various operating conditions of the inlet, a conical plug with a half-angle of 33.8 degrees was utilized, where as seen from Fig. 4 its maximum diameter was equal to the exit internal diameter of the cowl. The axial movement of plug assembly was responsible for controlling the outlet flow area and regulating the back pressure of the inlet. In this research, to create various back pressures, this plug has been simulated at the end of the inlet. In this regard, the Exit Blockage Ratio (EBR) is defined as a percentage according to Eq. (4) and Fig. 4:

$$EBR = \frac{h_{blocked}}{h_{exit}} \times 100 \qquad (4)$$

When the outlet is completely obstructed by the plug, the exit blockage ratio reaches its maximum value of 100 %. Conversely, in an unobstructed state, this coefficient decreased to its minimum value of 0 %.

Table 2 presents a summary of the supersonic inlet's operating modes along with relevant flow features and performance metrics, according to the values of EBR. While this table identifies the general subcritical regime as EBR>62.5 % and the buzz onset beyond EBR=67.5 %, the present study specifically investigates the EBR values starting at 64.0 %, covering conditions near and beyond the buzz onset.
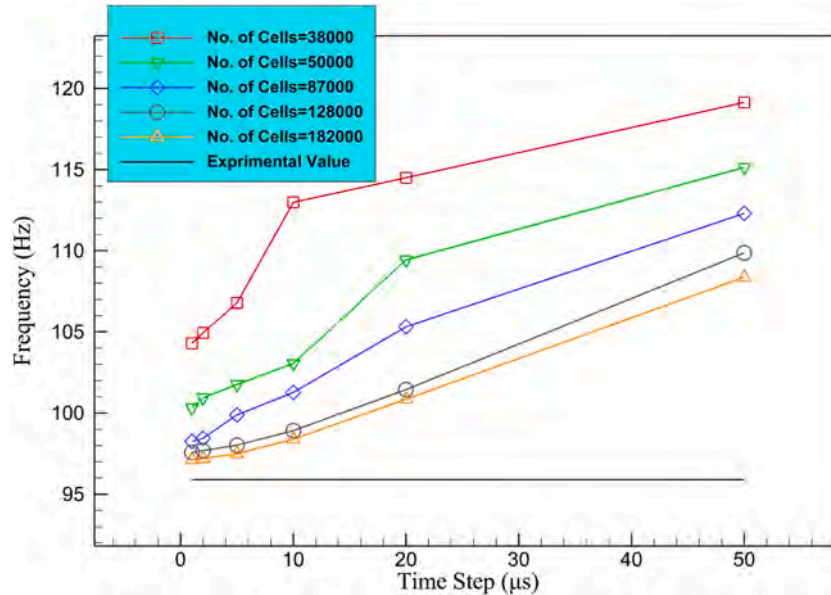

Fig. 8. Frequency of buzz oscillations at free-stream Mach number of 2 and EBR=70 % for various grid sizes and time steps.
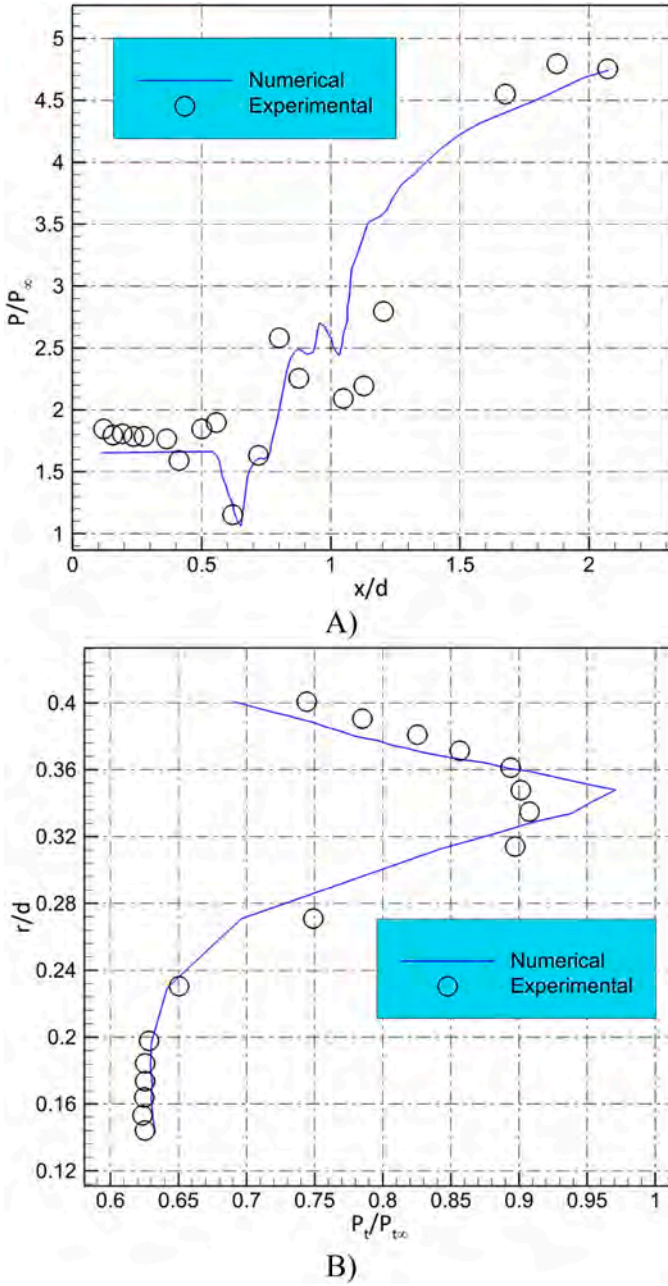
Fig. 9. Comparison of the numerical and experimental results at M_∞=2.0 and EBR=60 % (a supercritical and steady state condition), A) static pressure ratio on the spike surface, B) radial distribution of total pressure inside the inlet at x/d = 2.4.

Fig. 10. Comparison of the numerical and experimental results at M_∞=2.0 and EBR=70 % (a subcritical and unsteady condition), A) static pressure ratio on the spike surface at $t/T = 0.2$ as well as the numerical Mach number contours and experimental shadowgraph at this instant, B) static pressure ratio of sensor S8 during two cycles of buzz oscillations.

2.2. MRD configurations

Three MRD configurations have been examined in this study. In the first configuration, to create three cavities, two discs are embedded on the spike and the effects of these cavities have been investigated in three positions: left, centre, and right. Fig. 5 illustrates the geometric dimensions of the disk row and their respective positions in the first configuration. The meaning of 'd' in this figure is the maximum diameter of the inlet model as shown in Fig. 2. The situation where the disks are positioned at the centre of the spike tip is designated as the Centre. When the disks are shifted to the right, it is referred to as Right, and when it is shifted to the left, it is labeled as Left. The dimensions of the cavities in all three situations are similar. Based on previous studies [31] conducted under steady conditions (i.e., before the onset of wave
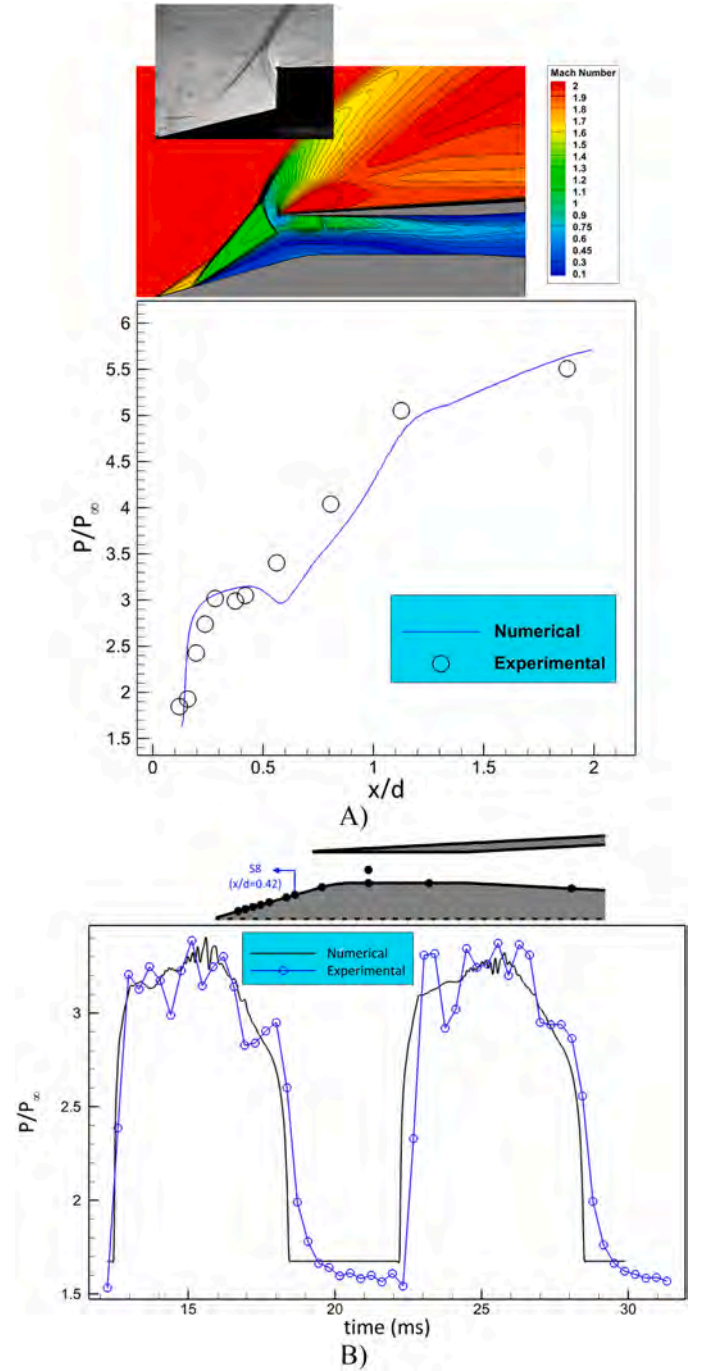
oscillations), and using a Design of Experiments (DOE) approach, it was found that the selected cavity depth and length caused the least negative impact on performance parameters and in some cases even improved them. Therefore, the same dimensions were used in this study to preserve the performance parameters under steady conditions as well. Although the present study focuses on instability and the buzz phenomenon, we deliberately adopted the optimized cavity dimensions identified in reference [31] to avoid adverse effects on performance parameters under steady conditions. For example, a further increase in cavity length and depth might be more effective in suppressing
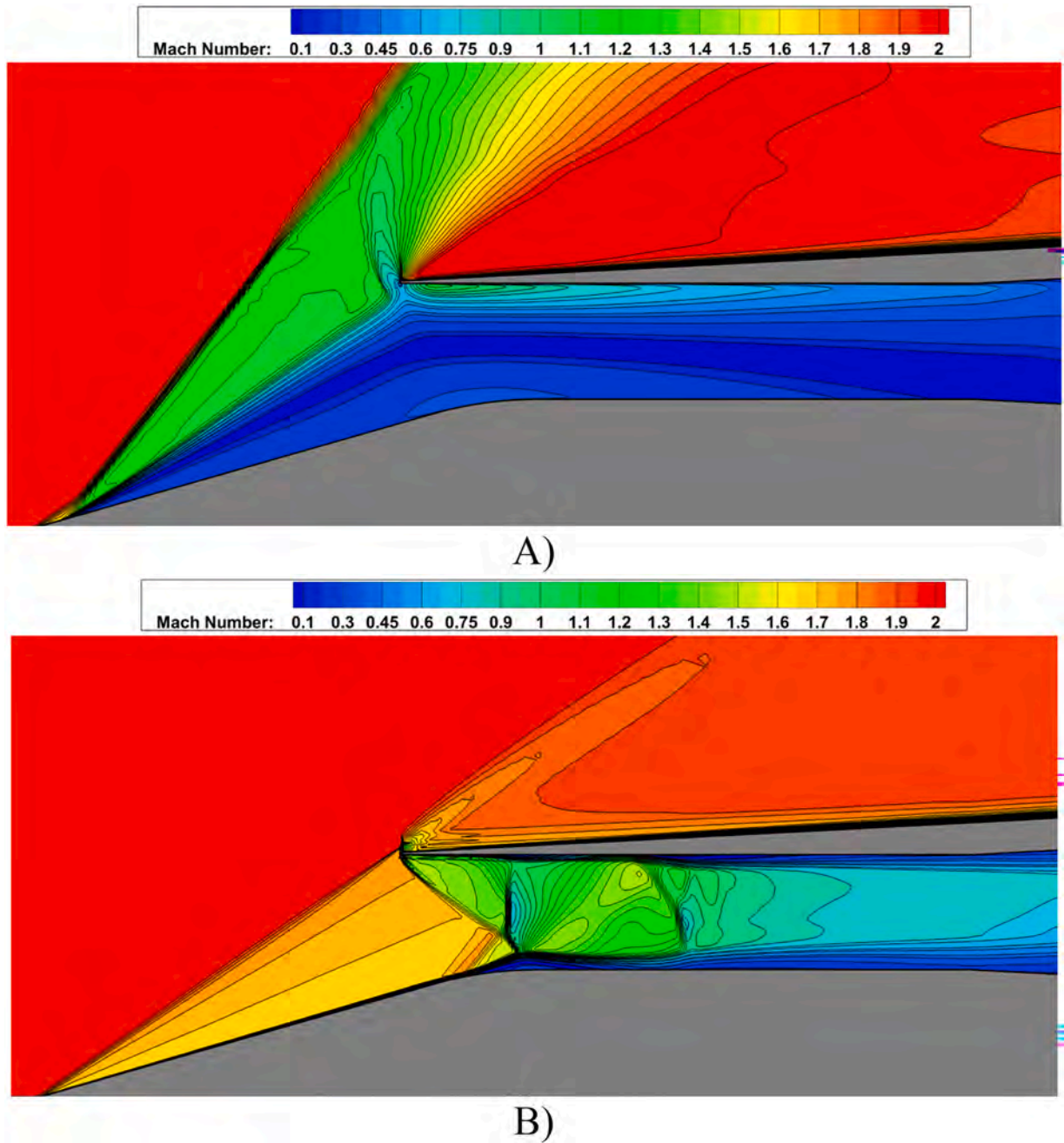
Fig. 11. Mach number contours for the base inlet without MRD at EBR=70 %, A) the upstream-most location of shock waves during the buzz oscillations, B) the downstream-most location of shock waves during the buzz oscillations.

buzz-related oscillations, but according to [31], increase in the cavity length and depth can significantly increase the drag coefficient of the inlet. Thus, in this study, a trade-off was made between suppressing buzz and maintaining acceptable performance.

Based on the numerical results gained from the previous configuration that will be explained later; to increase the effectiveness of the previous configuration, the second configuration covers the entire surface of the tip cone with multiple disks as shown in Fig. 6. In fact, as the inlet experiences various back pressures at the subcritical conditions, the position of the terminal normal shock varies significantly over the surface of the tip cone. Therefore, to reduce the separation region for a wider range of back pressures, more cavities are introduced in the second configuration. The length of all cavities is set to 0.04d, and the depth of them is variable according to their location. Additionally, the thickness of all disks is equal to 1 mm.

In the third configuration, to eliminate the dead flow within the cavities and further remove the separated region over the spike surface and increase the effectiveness of the MRD method, in addition to covering the entire surface of the spike with some disks, a discharge mechanism has been also applied. The geometry and dimensions of this configuration are illustrated in Fig. 7. Due to the significance of the downstream-most cavity, the height of the channel connected to this cavity is set to 3 mm, while the heights of the other channels are limited to 2 mm.

2.3. Grid and time step sizes

In addition to selecting the optimal grid size, choosing an appropriate time step is crucial for the computation of unsteady problems. The Fast Fourier Transform (FFT) is a powerful tool for obtaining the
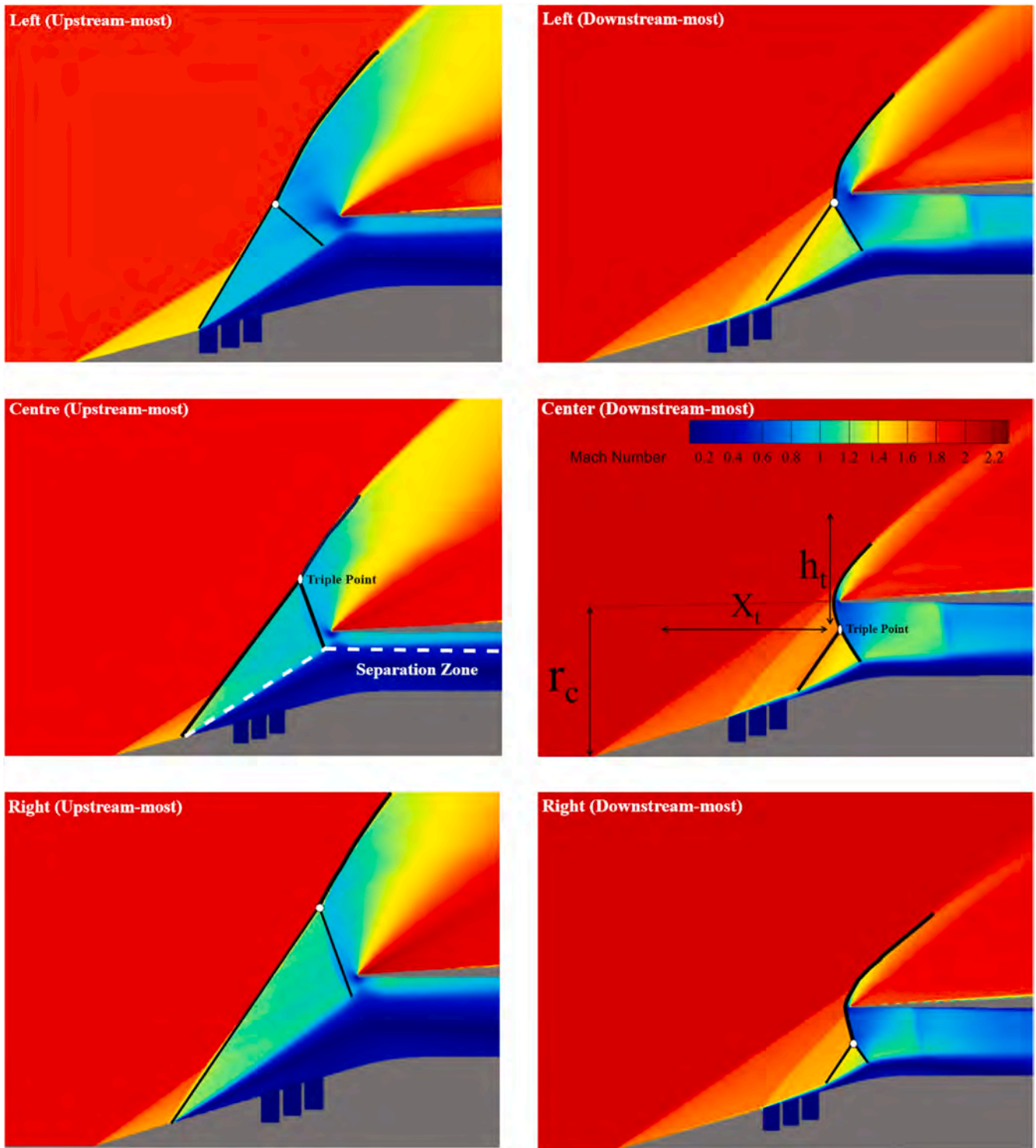
Fig. 12. Mach number contours for the first MRD configuration at EBR=70 %.

Table 3

Amplitudes of axial and radial oscillation of triple point and buzz dominant frequency at EBR=70 %.

Disk Position	Dominant Frequency (Hz)	h_t/r_c	X_t/r_c
Base (without disks)	96	–	–
Left	23	0.14	0.30
Centre	25	0.60	0.25
Right	26	0.69	0.23

dominant frequency of oscillatory phenomena and is utilized throughout various sections of this research. FFT is one of the most significant and widely used algorithms in the field of signal processing. Five different meshes were analyzed at six distinct time steps to find the frequency of the buzz oscillations at $M_\infty=2.0$ and EBR=70 % as seen in Fig. 8. According to this figure, the mesh with 128,000 cells and a time step of 5 microseconds are optimal.
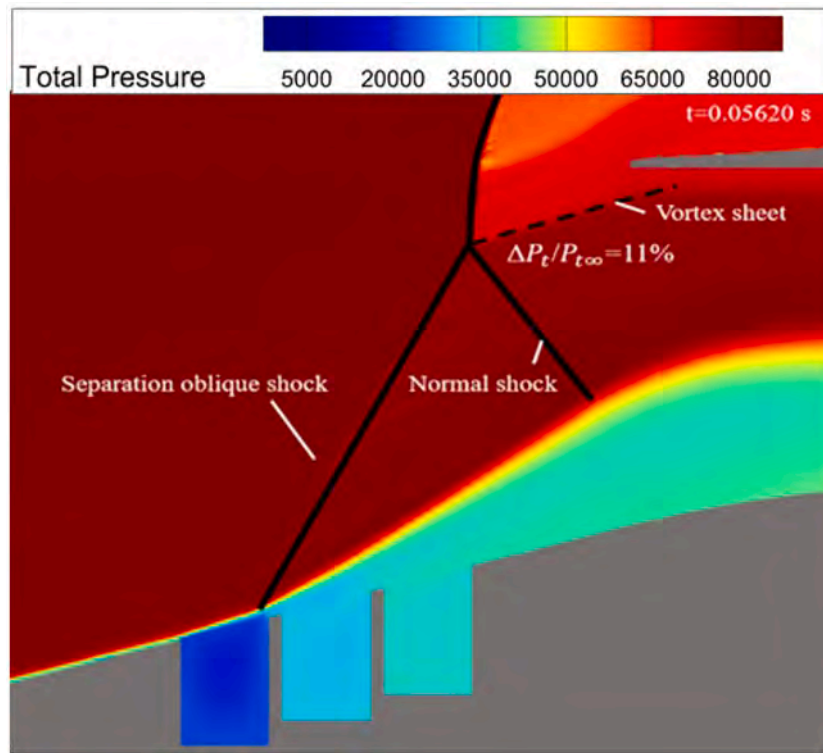
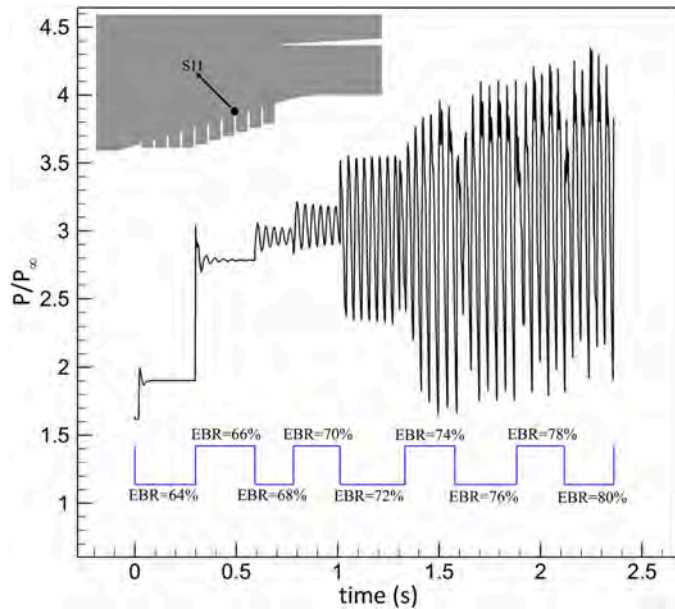**Fig. 13.** Total pressure contours in the Right situation at EBR=70 %.

Fig. 14. Pressure ratio of sensor S11 as a function of time for the second MRD configuration.

Fig. 15. Wave motion ranges and changes in the separation region thickness for the second MRD configuration.

2.4. Validation of the numerical results

To survey the accuracy of the numerical methodology in steady and unsteady states, the numerical results are compared with the results of wind tunnel testing of the current inlet [29,32]. As seen in Fig. 9, a satisfactory agreement is observed between the numerical results and the experimental data of static and total pressures in a steady case.

To validate the unsteady results, the instantaneous pressure over the spike during the buzz oscillations of EBR=70 % at $t/T = 0.2$ is demonstrated in Fig. 10A). In this figure, T is the period of the buzz cycle and the start of the buzz cycle is considered to be when the shock waves are at their upstream-most location near the spike tip. Additionally, the variations of static pressure of sensor S8 over time during two cycles of buzz oscillations are shown in Fig. 10B). As observed, the selected numerical methods can also accurately predict the experimental results in the unsteady operating conditions. To further confirm the numerical results, the experimental shadowgraph image is also presented to provide a direct comparison between the numerical and experimental results.

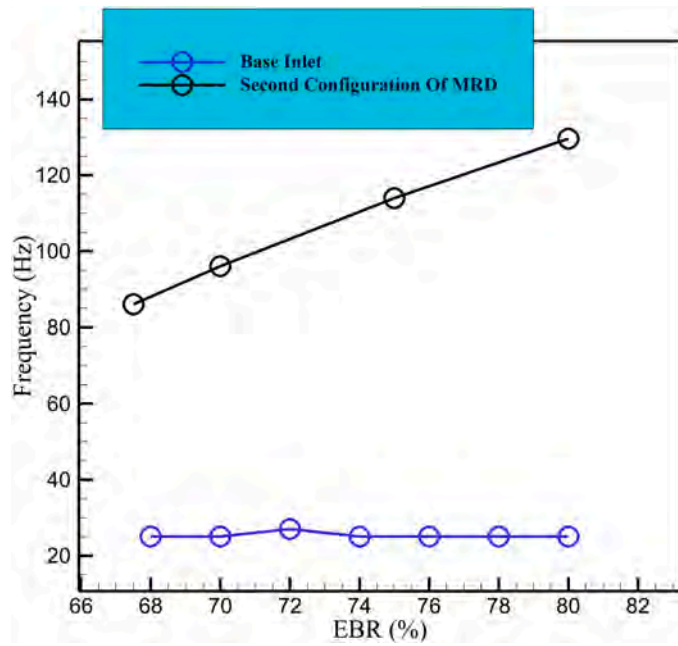**Fig. 16.** Dominant frequency of buzz oscillations for the base inlet and the second configuration of MRD.

Fig. 18. Variations of the inlet mass flow rate during buzz oscillations at EBR=70 %.
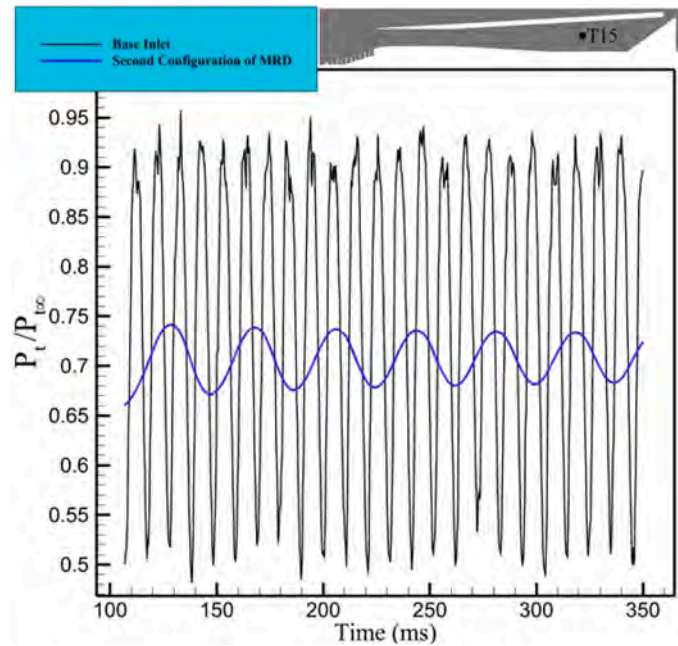

Fig. 17. Total pressure of sensor T15 as a function of time at EBR =70 %.

To validate the unsteady numerical results, the frequencies of buzz oscillations at two EBRs are compared with the experimental values. Based on Fig. 8, the numerical dominant frequency at EBR=70 % is about 98 Hz. According to the wind tunnel tests [29], the dominant frequency of oscillations at this EBR is 96 Hz, which is very close to the numerical value. In addition, at EBR=80 %, the dominant frequency is 127 Hz in experimental tests and 129.6 Hz in the numerical simulations.

3. Results and discussion

For the base inlet (without MRD) at free-stream Mach number of 2, the buzz phenomenon begins at EBR=67.5 % based on the Dailey
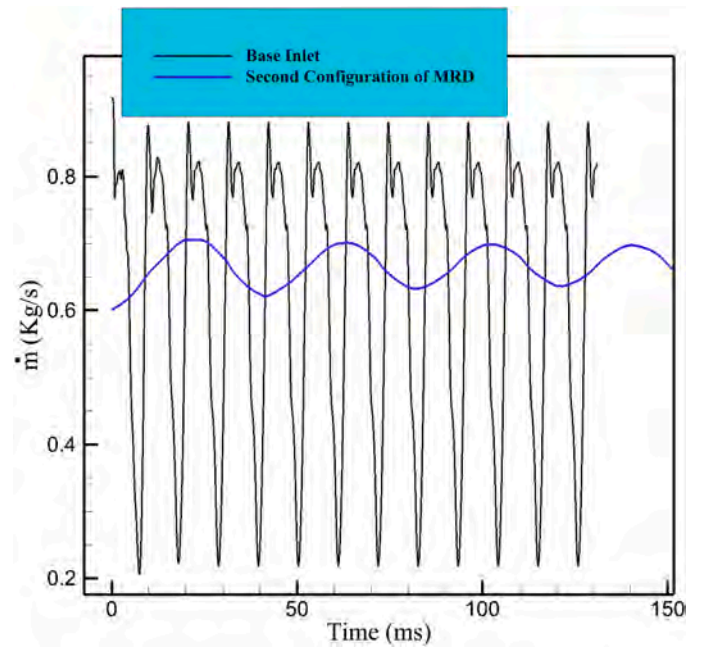
criterion [32]. The oscillation frequency at this EBR is 90 Hz. Increasing the exit blockage ratio to 70 % raises the frequency to 96 Hz [28]. For this blockage ratio, the set of shock waves during buzz oscillations reach near the spike tip at the upstream-most situation, as shown in Fig. 11A). At the downstream-most situation, they reach the inlet throat as seen in Fig. 11B). With a further increase in the exit blockage ratio to 75 % and 80 %, the oscillation frequency rises to 113 Hz and 127 Hz, respectively, and the amplitude of the shock wave oscillations also increases. In the upstream-most condition, the waves reach the spike tip, and in the downstream-most condition, they reach downstream of the throat inside the subsonic diffuser [29]. In the subsequent sections, the impacts of different MRD configurations on this flow behavior, as described here, will be examined.

3.1. First MRD configuration

For all three cases of the first MRD configuration, namely left, center, and right, the buzz starts at EBR=67.5 %, similar to the inlet without MRD. Therefore, this configuration does not delay the buzz onset. However, as shown in Fig. 12, the amplitude of the shock wave oscillations is smaller compared to the base inlet (Fig. 11), and the amplitude is confined to a region outside the inlet. Additionally, Table 3 indicates that using the first MRD configuration also reduces the oscillation frequency considerably.

According to Fig. 12, the presence of a normal shock wave outside the inlet generates a series of other shock waves, which include the normal shock wave itself, an oblique shock wave resulting from the separation caused by the interaction of the normal shock wave with the boundary layer, and a stronger shock wave that arises from the intersection of these two shock waves. The basis for calculating the oscillation amplitude of this series of waves is the triple point, which is where these waves intersect each other. While the triple point is always present in front of the inlet for the first MRD configuration, it does not exist in the base inlet as seen in Fig. 11.

The motion of shock waves during the buzz oscillations is divided into two components; axial and radial. As seen in Fig. 12, the axial motion of the wave series is represented by X_t, while the radial motion is denoted by h_t. Additionally, r_c represents the radius of the cowl lip. Ignoring the slight differences in the dominant frequencies, which are
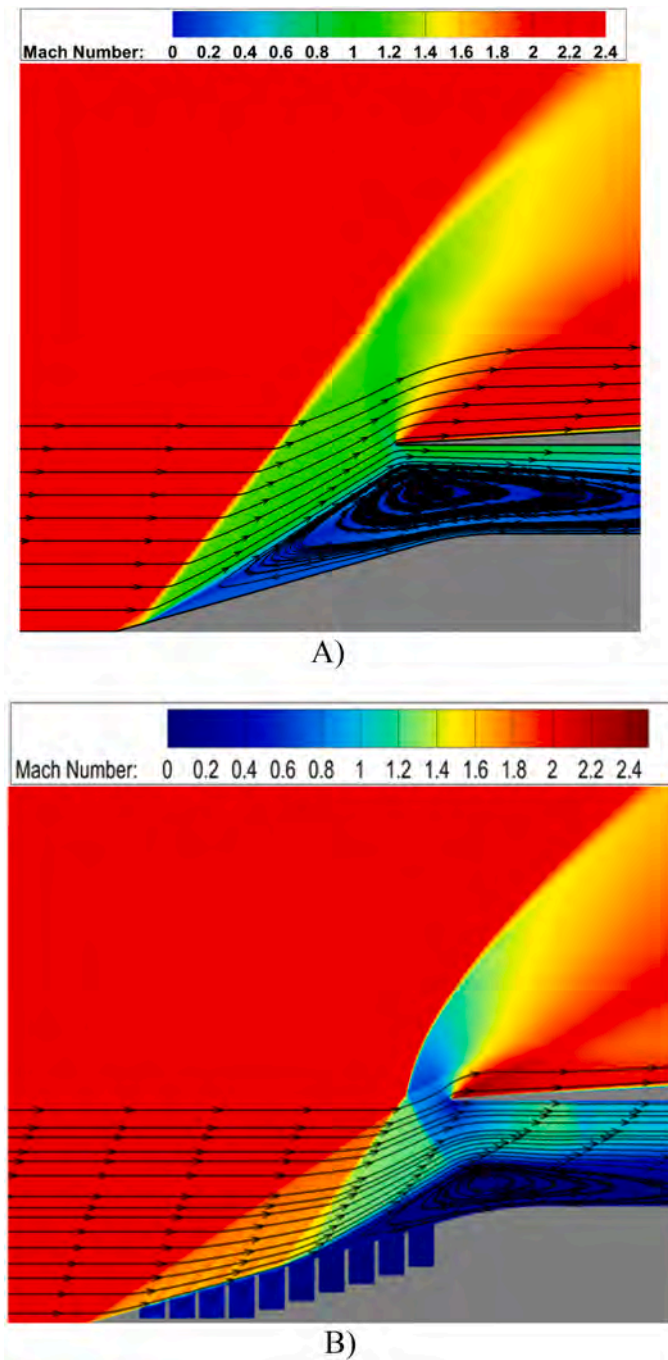
Fig. 19. Contours of Mach number and streamlines showing the height of separation region around the inlet entrance at EBR=70 %, A) base inlet at the upstream-most position of shock waves during the buzz oscillations, B) inlet with the second configuration of MRD.

Fig. 20. Static pressure variations of sensor S11 at EBR=72%.

3.2. Second MRD configuration

The second configuration, the case in which the entire surface of the tip cone is covered with cavities, has been examined with exit blockage ratios ranging from 64 % to 80 % by a step of 2 %. According to Fig. 14, no oscillations are observed at EBR=64 %. At EBR=66 %, slight oscillations occur, which are completely damped due to the presence of the cavities. At EBRs of 68 % and 70 %, oscillations with low amplitude and a frequency similar to the frequency at higher exit blockage ratios are observed. These oscillations are local and their source is the oscillations of separation bubble, which do not constitute the buzz phenomenon. In the base inlet, similar oscillations are observed at EBR=65 % before the buzz onset [32]. In studies [34,35], terms such as mixed buzz, medium buzz, or pre-buzz onset oscillations are used to mention this phenomenon. These conditions indicate a transition from stability toward instability of the inlet and the buzz initiation. In EBRs of 68 % and 70 %, separation covers almost half of the throat height. Based on the pressure variations shown in Fig. 14, it appears that the onset of the buzz phenomenon occurs at EBR=72 % which is approximately 4.5 % more than the base inlet without MRD.

With the increase in the number of disks in the second MRD configuration, the range of shock motion has significantly decreased as compared with the base inlet and with the first MRD configuration. The cause of the axial oscillation of the waves during the buzz phenomenon is the increase and decrease in the amount of flow spillage around the cowl lip, which occurs due to the flow choking at the throat. Fig. 15 illustrates the amplitude of axial movement, radial movement amplitude, and separation height at the throat. From EBR=74 % and above, separation at its maximum extent covers the entire height of the throat; therefore, the value of r_s/r_t remains constant and is equal to 1.0, where r_s is the maximum height of the separation region from the spike surface and r_t is the total height of the throat duct. When the wave system reaches its highest position, it transforms into a bow shock. Under these conditions, the triple point disappears, and the amplitude of radial wave motion cannot be calculated; hence, the value of h_t/r_c is not presented for blockage ratios above 72 % in Fig. 15. The calculated amplitudes for the axial motion of the waves at EBR=74 % and above are approximate

shown in Table 3, as the disks approach the inlet entrance, the amplitude of the axial oscillations decreases while the radial motion is amplified.

In all three situations, the primary factor for the buzz onset is based on the Dailey criterion, which pertains to the separation of flow over the spike surface. However, in the Right condition, as illustrated in Fig. 13, the vortex sheet generated from the intersection of normal and oblique shock waves collides with the inner surface of the cowl. Given that the total pressure difference across the vortex sheet is >7 % compared to the total pressure of the free stream, in this case, the buzz phenomenon can also commence according to the Ferri criterion [33].
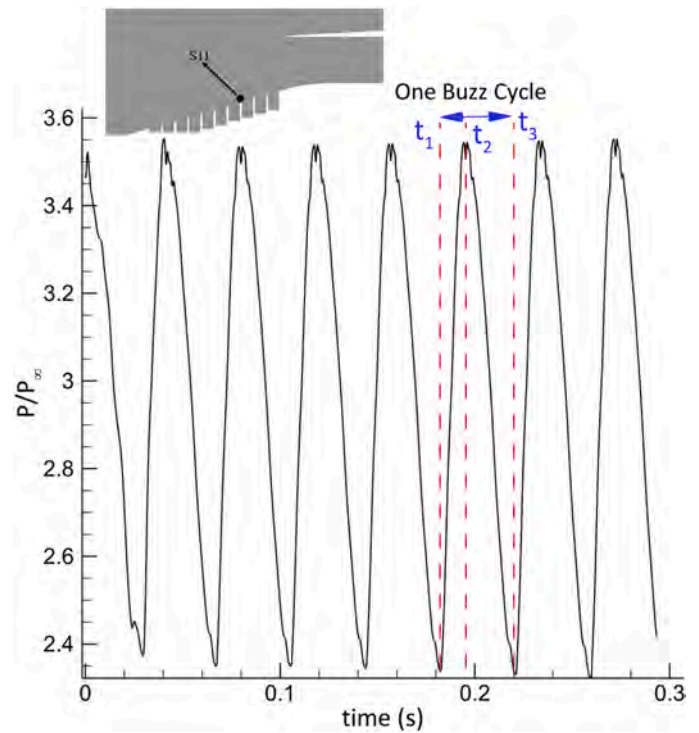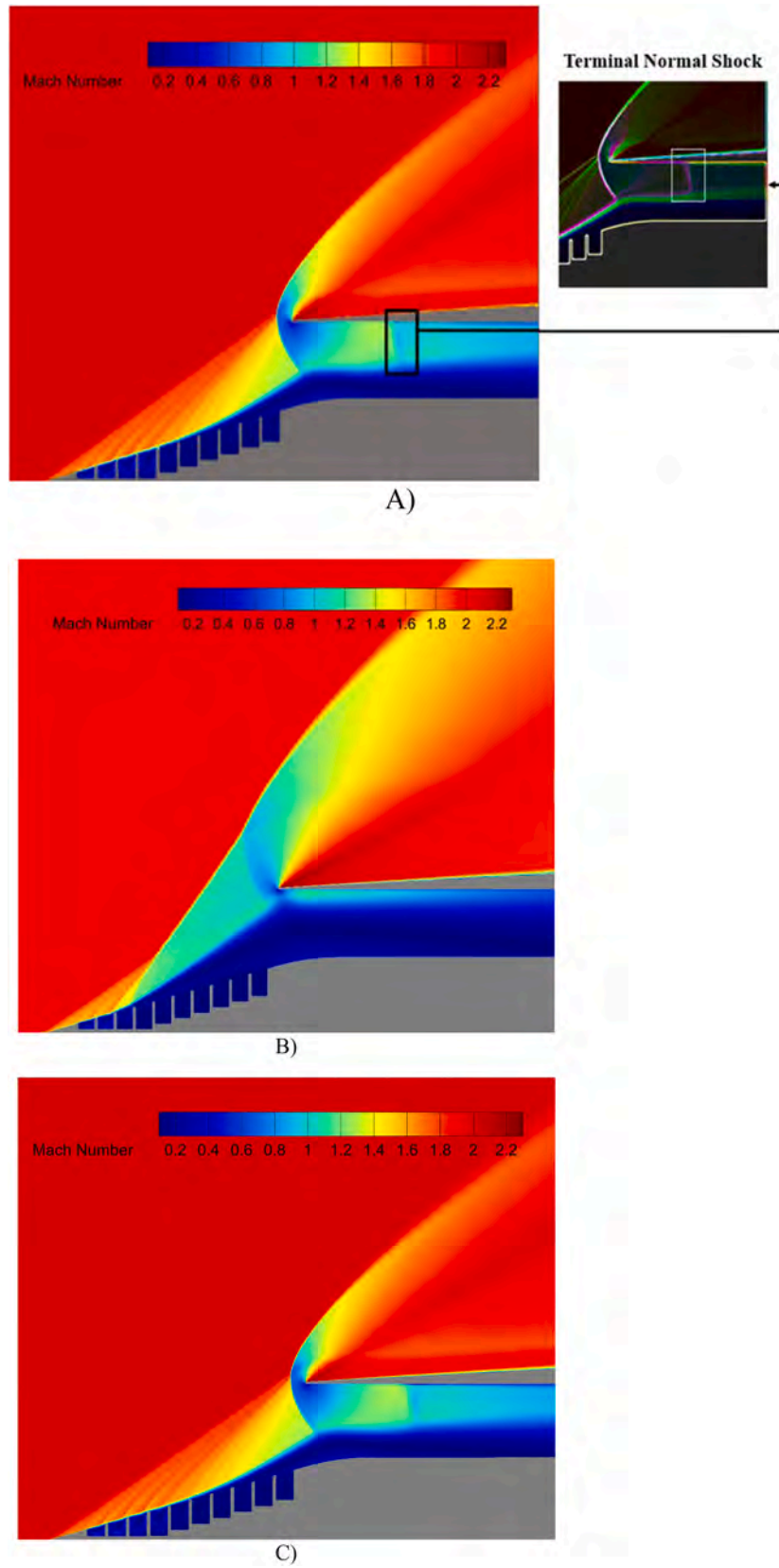
Fig. 21. Contours of Mach number for the second MRD configuration during the buzz oscillations at EBR=72 %, A) downstream-most location at t_1, B) upstream-most location at t_2, C) downstream-most location at t_3.
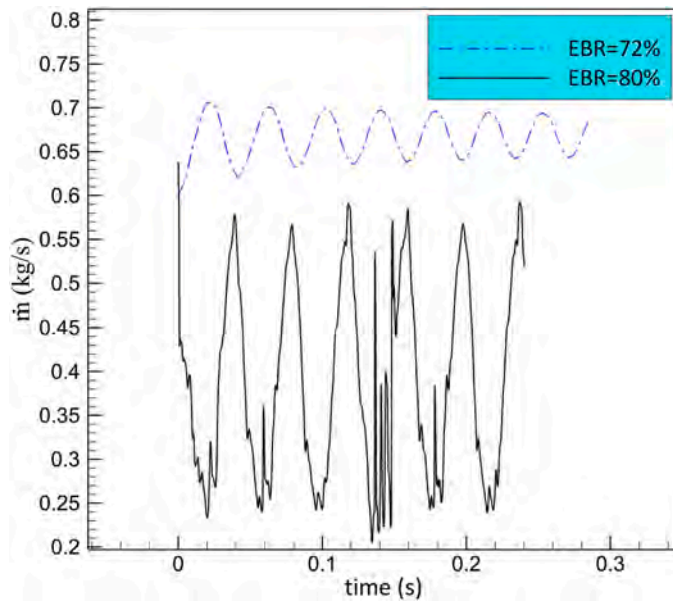
Fig. 22. Mass flow rate passing through the inlet during the buzz oscillations.

due to the loss of the triple point. However, because of the importance of these values during the buzz phenomenon, their values are shown in Fig. 15. In fact, when the wave system is in the upstream-most position, a point on the shock system is considered, whose height is similar to the height of the triple point when the set of waves is in the downstream-most position, and the axial distance between these two points is considered to be X_t. At EBR=74 %, cavities cannot remove a wide separation region, leading to the complete flow choking in the throat section. This occurrence results in a relatively sharp increase in the axial motion amplitude as seen from Fig. 15.

As seen from Fig. 16, for all exit blockage ratios examined for the second MRD configuration, the dominant frequency of oscillations is about 25 Hz, except for EBR=72 %, where the dominant frequency is 27 Hz. In addition, this figure shows that there is a considerable reduction in the frequency of oscillations for the second configuration as compared with the base inlet.

The total pressure of the flow at the inlet end is one of the most important parameters of the inlet because its change is directly related to the change in the vehicle thrust. To study the effects of MRD on total pressure, data from sensor T15 has been utilized. Fig. 17 illustrates the total pressure variations over time at EBR=70 % for this sensor. As seen, the amplitude of total pressure fluctuations has significantly decreased in the presence of MRD, indicating that the MRD method has a great
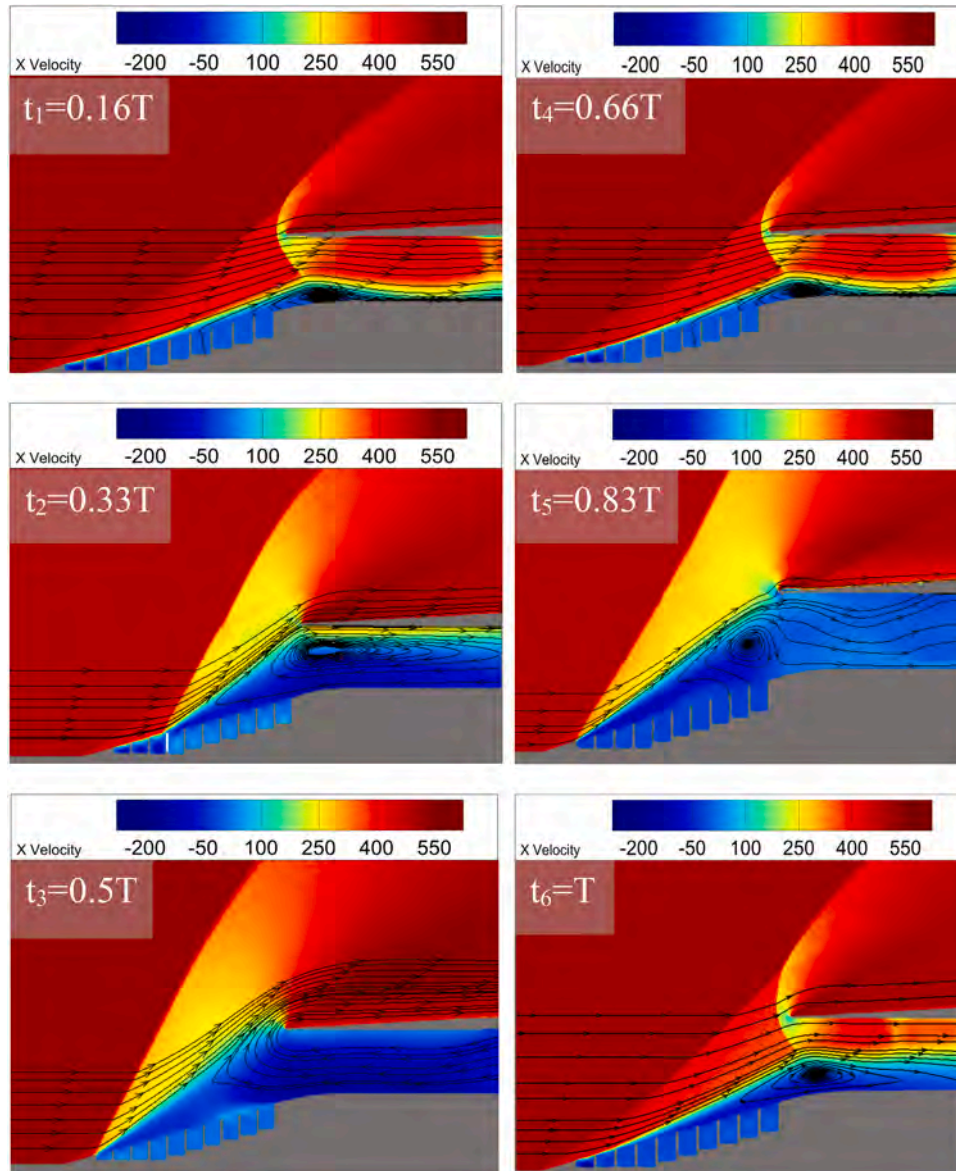

Fig. 23. Axial velocity contours and streamlines during one buzz cycle at EBR=80%.
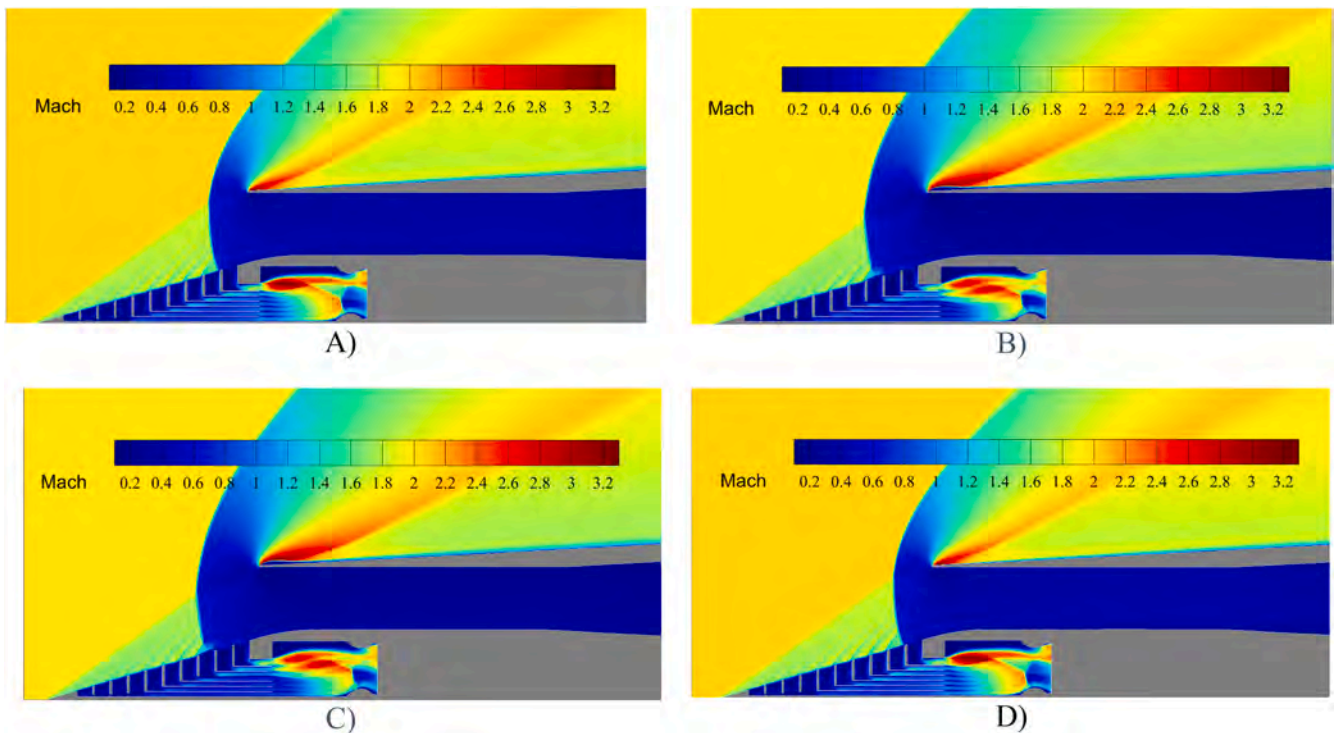
Fig. 24. Mach number contours for third MRD configuration, A) EBR=76 %, B) EBR=80 %, C) EBR=84 %, D) EBR=88 %.

impact on total pressure stability.

The mass flow rate passing through the inlet is another crucial parameter in the performance of inlets. The buzz phenomenon causes fluctuations in the mass flow rate of the inlet, which can degrade the engine performance seriously. Fig. 18 shows the inlet mass flow rate as a function of time at EBR=70 %. As observed, the minimum mass flow rate during buzz oscillations increases by about three times with the application of MRD, from 0.2 to approximately 0.6.

The reason for the aforementioned stabilizing effects of the MRD is the capability of this method in removing or at least decreasing the separation regions. By examining the Mach number contours in Fig. 19, it can be observed that the amount of separation at the throat has decreased in the presence of the cavities. Additionally, the separation shock wave is located near the middle of the spike tip cone, in contrast to the base inlet, where this shock wave is almost at the tip cone.

3.2.1. Description of the buzz cycle at EBR=72 %

One cycle of buzz oscillations at EBR=72 % is described here from t_1 to t_3 using Fig. 20. At time t_1, the wave set is positioned at the downstream-most location. Before t_1, the subsonic flow behind the shock system moving downstream accelerates in the throat and becomes supersonic. After traveling a distance, due to the back pressure at the inlet end, a normal shock wave forms in the throat at t_1 as shown in Fig. 21A), causing the flow to revert to subsonic conditions. At this time, the normal shock is located at its closest point to the throat during the buzz cycle. The separation region behind the normal shock is local and has limited effects. Spillage is at its minimum value, and consequently, both the inlet mass flow rate and exit total pressure are at their maximum values at this time. The high pressure flow inside the inlet forces the normal shock to move upstream between times t_1 and t_2. According to the Dailey criterion, the separation region enlarges and leads to increased spillage in front of the cowl and both the mass flow rate and total pressure inside the inlet decrease. At time t_2, as shown in Fig. 21B), the normal shock reaches its upstream-most position during a buzz cycle. Due to the large separation region caused by the interaction of the normal shock with the boundary layer, the main flow in the throat

is confined to a narrow converging channel near the inner surface of the cowl, where the flow becomes highly concentrated. The limited flow area in this condition leads to a minimum inlet mass flow rate. Low mass flow rate and low total pressure inside the inlet cause the separation region to be swallowed into the inlet [32], and during the time interval from t_2 to t_3, the normal shock moves downstream toward the inlet entrance. As the spillage region decreases, mass flow rate and total pressure inside the inlet increase. According to Fig. 21C), at time t_3, the normal shock is located at a position very close to its location at t_1. Therefore, the flowfield at t_3 is similar to that at t_1, as illustrated in Fig. 21A). This condition causes the shock wave to move upstream again, thus completing one buzz cycle.

3.2.2. Description of the buzz cycle at EBR=80%

With the increase of EBR, the amplitude of oscillations rises, leading to enhanced fluctuations in the mass flow rate within the inlet. Fig. 22 presents a comparison of mass flow rates at EBR levels of 72 % and 80 %. When the normal shock is at its upstream-most position, a sharp drop in the mass flow rate, accompanied by a sudden and temporary decrease in inlet pressure, causes the flow to be drawn into the inlet with a higher acceleration compared to the case with EBR=72 %.

A complete cycle of the buzz phenomenon at an EBR of 80 % is presented below using velocity contour plots. Since the buzz cycle generally follows a similar pattern across different EBR values, this section provides a general description of the phenomenon, with particular emphasis on the effect of increasing the EBR) or more specifically, the back pressure(which amplifies the amplitude and intensity of the oscillations. At the beginning of the cycle (t_1=0.16T), when the shock system is at its downstream-most position, the presence of a normal shock near the inlet entrance induces local flow separation and reattachment, as shown in Fig. 23. As the shock waves move upstream and the separation area expands, the wave system transforms into a single separation shock wave (t_2=0.33T). When this wave reaches the upstream-most cavity, the separation region covers the entire height of the throat, completely blocking the inlet and temporarily reversing the internal flow direction (t_3=0.5T). Shortly after (t_4=0.66T), the
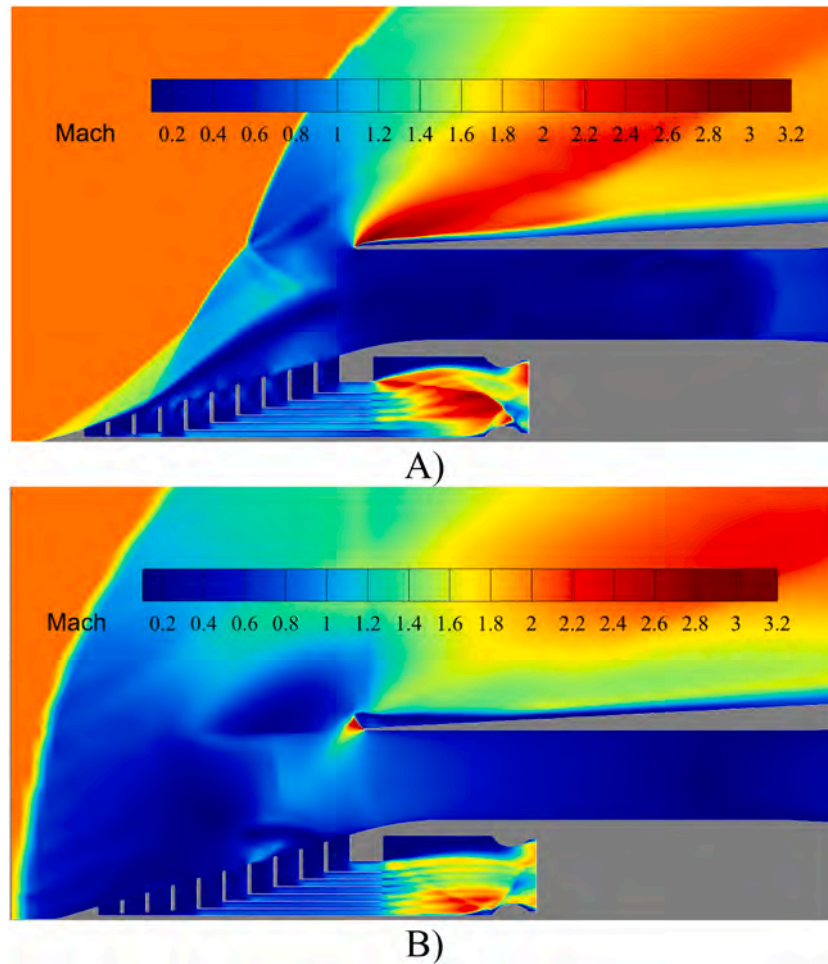
Fig. 25. Contours of Mach number at EBR=90 % for third MRD configuration, A) the downstream-most position of shock waves during the oscillations, B) the upstream-most position of shock waves during the oscillations.
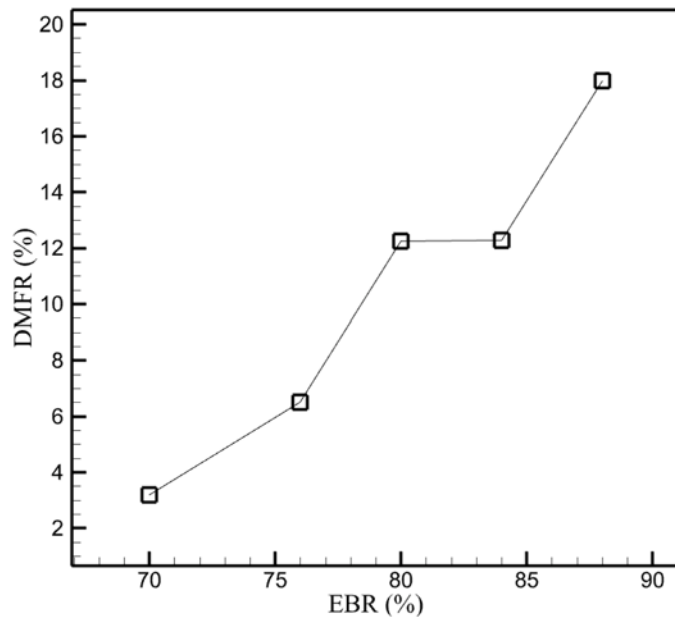

Fig. 26. DMFR values at various EBRs.

Table 4

Summary of stability ranges and onset of buzz for different MRD geometric configurations under various EBR's.

Geometric Configurations	Stability Range	Subcritical Stable Range	Onset of Buzz
First MRD Configuration	EBR< 62.5 %	–	EBR= 67.5 %
Second MRD Configuration	EBR≤ 66 %	62.5 % <EBR≤ 66 %	EBR= 72 %
Third MRD Configuration	EBR< 90 %	62.5 % <EBR< 90 %	EBR= 90 %

separation shock wave undergoes strong unsteady oscillations locally at the tip. The discharge of the inlet mass flow from the entrance, combined with the sharp reduction in pressure and mass flow rate inside the inlet, causes the separation region to be sucked into the inlet, and the shock wave system moves downstream again. At t_s=0.83T, the shock system is drawn further downstream, allowing fresh air to re-enter the inlet. At t_e=T, the buzz cycle is completed, and the shock system reaches its downstream-most position again.

As this analysis shows, the expansion and contraction of the separation region on the spike surface have a significant impact on the creation and continuation of buzz oscillations. Therefore, covering the entire spike tip cone with a series of cavities using the MRD method greatly helps in reducing the intensity of buzz oscillations and

controlling its characteristics.

3.3. Third MRD configuration

As shown in the previous section, despite covering the entire surface of the spike tip with a series of cavities, the separation region becomes so large that it covers the entire height of the inlet throat. This causes the flow direction inside the inlet to be completely reversed for a very short time during the buzz phenomenon. Therefore, in the third MRD configuration, a discharge mechanism is inserted inside the spike. With the implementation of this mechanism, the separation region on the spike can be eliminated, and the shock wave oscillations can be suppressed. According to Fig. 24, as EBR increases up to 88 %, the flow field is completely stable and there are no buzz oscillations.

The MRD of the third configuration has delayed the buzz onset until EBR=90 %, which shows a 22.5 % increment as compared with the base inlet. According to Fig. 25, at EBR=90 %, the buzz oscillations suddenly begin with irregular amplitudes and various frequencies. The amplitude of oscillations and separation region height increase to such an extent that a detached shock wave is formed in front of the spike and the discharge mechanism is unable to eliminate the large volume of separation. As a consequence of this large separated region, when the shock waves are located at their downstream-most position, a significant portion of the incoming flow spills around the cowl lip. As the flow passes over the curved cowl lip, it accelerates and expands, resulting in reduced static pressure and increased Mach number. This explains the high-velocity region observed over the cowl surface in part A) of Fig. 25. In addition, when the shock waves shift to their upstream-most position, the direction of flow inside the inlet throat is instantly reversed before spilling again over the cowl lip. As depicted in part B) of Fig. 25, this leads to further acceleration and expansion of the flow around the cowl lip, producing a high Mach number region near the cowl lip and a separation zone along the upper cowl wall.

To investigate the amount of mass flow rate for the discharge mechanism, a parameter defined as Discharged Mass Flow Ratio (DMFR) is used. This parameter is the ratio of the mass flow rate exiting the discharge nozzle to the mass flow rate entering the inlet. As seen from Fig. 26, an increase in EBR leads to a higher DMFR value. The maximum value corresponds to EBR=88 %, which is the last stable EBR and does not exceed 20 %. Although this amount seems large, it should be noted that the discharged mass flow can be re-entered into the engine or used for the cooling purposes. In addition, in the absence of this discharge mechanism, the buzz phenomenon occurs during which the mass flow rate experiences significantly lower values along with severe fluctuations.

Table 4 summarizes the range of stability, the range in which the shock waves remain stable under subcritical conditions, and the onset of buzz for different MRD geometric configurations used in this study under various EBR conditions.

4. Conclusions

In this study, a supersonic axisymmetric inlet with mixed compression was numerically studied at the free stream Mach number of 2. The accuracy of the numerical model was validated by comparing the results with experimental data from wind tunnel tests of the current inlet. Subsequently, the MRD method was applied to the surface of the spike in three configurations to delay the onset of buzz oscillations. As the first configuration, two disks (three cavities) were placed on the spike tip cone, and their effects on the buzz characteristics were investigated. Based on the observations, two disks were found insufficient to postpone the buzz phenomenon, only succeeding in reducing the frequency and amplitude of oscillations. Increasing the number of disks so that they covered entire surface of the spike tip in the second configuration led to the buzz onset postponement to an exit blockage ratio 4.5 % greater than the base inlet. The oscillation frequency remained constant at about 25

Hz for all blockage ratios in the second MRD configuration, which is approximately one fourth of the value for the base inlet. Comparative analysis revealed significant reductions in total pressure and mass flow rate fluctuations due to the implementation of MRD. The investigation of one buzz cycle in the second configuration indicated that while MRD can postpone the buzz onset and alleviate the adverse effects of the buzz oscillations, it needs a discharge mechanism to further eliminate the separation region at higher exit blockage ratios. Combining MRD with the discharge mechanism can delay the buzz onset up to an exit blockage ratio, which is 22.5 % greater as compared with the base inlet. The findings of this research demonstrated that the MRD method is an efficient and straightforward approach for improving the inlet stability.

CRediT authorship contribution statement

Sohrab Panahandeh Taghi-Abad: Writing – original draft, Data curation. **Mohammad Hossein Moghimi Esfand-Abadi:** Writing – review & editing, Validation, Data curation. **Javad Sepahi-Younsi:** Validation, Supervision, Project administration, Methodology, Conceptualization.

Declaration of competing interest

The authors declare that they have no known competing financial interests or personal relationships that could have appeared to influence the work reported in this paper.

Data availability

No data was used for the research described in the article.

References

[1] E.L. Goldsmith, J. Seddon, Practical Intake Aerodynamic Design, Blackwell Scientific Publications, London, 1993.

[2] G.C. Oates, Aircraft Propulsion Systems Technology and Design, AIAA, 1989.

[3] K. Hünecke, Jet engines: Fundamentals of theory, design, and Operation, MotorBooks International Publishers and Wholesalers, 1997.

[4] Y. Choe, C. Kim, K. Kim, Effects of optimized bleed system on supersonic inlet performance and buzz, J. Propuls. Power. 36 (2) (2020) 211–222.

[5] J.D. Anderson, Hypersonic and High Temperature Gas Dynamics, 2nd ed., AIAA, Reston, VA, 2006.

[6] S. Trapier, P. Duveau, S. Deck, Experimental study of supersonic inlet buzz, AIAA Journal 44 (10) (2006) 2354–2365.

[7] R.V. Chima, Analysis of Buzz in a Supersonic Inlet, NASA/TM—2012-217612, 2012.

[8] K. Ye, X. Zhou, Z. Ye, Buzz characteristics under fluid–Structure interaction of variable-geometry lip for hypersonic inlet, AIAA Journal 62 (5) (2024) 1662–1682.

[9] A. Ferri, L.M. Nucci, The Origin of Aerodynamic Instability of Supersonic Inlets At Subcritical Conditions, NACA RM-L50K30, 1951.

[10] C.L. Dailey, Supersonic diffuser instability, J. Aeronaut. Sci. 22 (11) (1955) 733–749.

[11] Y. Zhang, H.-J. Tan, J.-F. Li, N. Yin, Control of cowl-shock/boundary-layer interactions by deformable shape-memory alloy bump, AIAA Journal 57 (2) (2019) 696–705.

[12] J. Shigematsu, K. Yamamoto, K. Shiraishi, A. Tanaka, A numerical investigation for supersonic inlet with throat cavity, in: 27th Joint Propulsion Conference, 1991.

[13] M. Vyas, S. Hirt, R. Chima, D. Davis, T. Wayman, Experimental investigation of micro vortex generators on a low boom supersonic inlet, in: 29th AIAA Applied Aerodynamics Conference, 2011.

[14] R. Jagannathan, W.S. Hinman, C. Johansen, Performance assessment of supersonic and hypersonic intake systems with nano-particle injection, Acta Astronaut. 159 (2019) 609–621.

[15] S.R. Maadi, J. Sepahi-Younsi, Effects of bleed type on the performance of a supersonic intake, Exp. Therm. Fluid. Sci. 132 (2022) 110568.

[16] J. Sepahi-Younsi, S. Esmaeili, Source of buzz instability in a supersonic air inlet, Aerosp. Sci. Technol. 138 (2023) 108334.

[17] H. Chen, H.-j. Tan, Y.-z. Liu, Q.-f. Zhang, External-compression supersonic inlet free from violent buzz, AIAA Journal 57 (6) (2019) 2513–2523.

[18] H. Kobayashi, N. Tanatsugu, T. Sato, Y. Maru, T. Kojima, Experimental study of multi-row disk inlets for hypersonic air breathing propulsion, in: 42nd AIAA Aerospace Sciences Meeting and Exhibit, Reno, Nevada, American Institute of Aeronautics and Astronautics, 2004.

[19] Y. Maru, N. Tanatsugu, T. Sato, H. Kobayashi, T. Kojima, K. Okai, Multi-row disk arrangement concept for spike of axisymmetric air inlet, in: 40th AIAA/ASME/

SAE/ASEE Joint Propulsion Conference and Exhibit, Fort Lauderdale, Florida, American Institute of Aeronautics and Astronautics, 2004.

[20] H. Kobayash, Y. Maru, M. Hongoh, S. Takeuchi, K. Okai, T. Kojima, Study on variable-shape supersonic inlets and missiles with MRD device, Acta Astronaut. 61 (11–12) (2007) 978–988.

[21] Y. Maru, H. Kobayashi, S. Takeuchi, T. Sato, Flow oscillation characteristics in conical cavity with multiple disks, J. Spacecr. Rockets. 44 (5) (2007) 1012–1020.

[22] S.E. Vali, S. Abbasi, Hypersonic drag and heat reduction mechanism of a new hybrid method of spike, multi-row discs and opposing jets aerodynamic configuration, Int. J. Heat. Mass Transf. 194 (2022) 123034.

[23] J. Sinha, S. Singh, O. Prakash, D. Panchal, Design optimization of a multi row disk inlet device with an optimum nose cone angle, FME Trans. 51 (2023) 23–30.

[24] M. Soltani, J. Younsi, M. Farahani, Investigation of a new flux scheme for the numerical simulation of the supersonic intake flow, Proc. Inst. Mech. Engineers Part G 226 (11) (2012) 1445–1454.

[25] M.R. Soltani, J.S. Younsi, M. Farahani, A. Masoud, Numerical simulation and parametric study of a supersonic intake, Proc. Inst. Mech. Eng. Part G 227 (3) (2013) 467–479.

[26] M. Soltani, J. Sepahi Yoinsi, V. Farajpoor Khanaposhtani, Numerical investigation of the unstart suppression in a supersonic air intake, Iranian J. Sci. Technol. Trans. Mech. Eng. 39 (M2) (2015) 413–426.

[27] J. Sepahi-Younsi, S. Esmaeili, Performance enhancement of a supersonic air intake by applying a heat source, J. Aerosp. Eng. 33 (5) (2020) 04020048.

[28] M. Soltani, M. Farahani, J.S. Younsi, Performance study of a supersonic inlet in the presence of a heat source, Scientia Iranica 18 (3) (2011) 375–382.

[29] J. Sepahi-Younsi, Effects of boundary-layer bleed parameters on supersonic intake buzz, Aerosp. Sci. Technol. 120 (2022) 107246.

[30] J. Sepahi-Younsi, Experimental study of the buzz phenomenon in a supersonic inlet with and without the bleed, Aerosp. Sci. Technol. 163 (2025) 110346.

[31] M. Naturizadeh, J. Sepahi-Younsi, Effects of MRD concept on the performance of a supersonic air inlet, J. Aeronaut. Eng. 26 (1) (2024) 135–148 (In Persian).

[32] M.R. Soltani, J. Sepahi-Younsi, Buzz cycle description in an axisymmetric mixed-compression air intake, AIAA Journal 54 (3) (2016) 1040–1053.

[33] S. Fisher, M. Neale, A. Brooks, On the Sub-Critical Stability of Variable Ramp Intakes At Mach Numbers Around 2, National Gas Turbine Establishment Rept. ARC-R/M-3711, Fleet, England, U.K., 1970.

[34] H. Chen, H. Tan, Y. Liu, Q.-f. Zhang, External-compression supersonic inlet free from violent buzz, AIAA Journal 57 (6) (2019) 2513–2523.

[35] H. Chen, H.-j. Tan, Buzz flow diversity in a supersonic inlet ingesting strong shear layers, Aerosp. Sci. Technol. 95 (2019) 105471.